THE JOURNAL OF PHYSICAL CHEMISTRY B

Article

pubs.acs.org/JPCB

# Water Gradient in the Membrane–Water Interface: A Time-Resolved Study of the Series of *n*-(9-Anthroyloxy) Stearic Acids Incorporated in AOT/Water/iso-octane Reverse Micelles

Michel Vincent* and Jacques Gallay

Institut de Biochimie et de Biophysique Moléculaire et Cellulaire, Université Paris-Sud, UMR 8619-CNRS, F-91405 Orsay, France

**ABSTRACT:** The water radial distribution in AOT/iso-octane/water reverse micelles (RM), used to mimic the membrane–water interface, was examined by excited-state lifetime and transient spectral measurements of the series of *n*-(9-anthroyloxy) stearic acids (*n*-AS), with *n* = 2, 3, 6, 7, 9, 10, and 12. A water gradient in the RM extended from the polar head group region up to the middle of the surfactant carbon chains. A fast intramolecular excited-state relaxation, involving the rotation of the carboxylic group of the ester bond with respect to the anthracene ring, gave rise to a nanosecond time-dependent fluorescence Stokes shifts (TDFSS). In water-filled RMs, we only observed a water-induced TDFSS occurring over subnano- and nanosecond time scales with decreasing amplitudes and rates as a function of depth, according to the decreasing water gradient and the slowing down of the anthroyloxy moiety rotational motion. This water-induced TDFSS is most likely the result of both H-bond formation and general dipolar relaxation, as indirectly showed by measurements with DMF (a nonprotic polar solvent) instead of water in RMs.

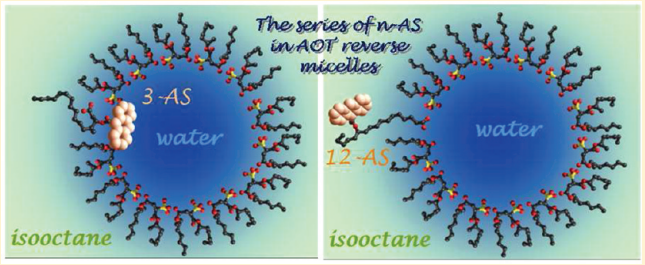


## INTRODUCTION

Biological membranes are complex two-dimensional dynamic assemblies of lipids and proteins whose physical and chemical properties (molecular composition, polarity, extent of water penetration, rotational mobility, acyl chain ordering) are depth-dependent. In particular, the polarity profile across cellular membranes is a key determinant of the interaction and insertion of proteins and bioactive peptides, which are affected by hydration state, local proton activity, hydrogen-bond availability, and lipid dynamics and ordering.[1] The polarity profile results from the distribution of the molecular constituents throughout the membrane–water interface, particularly water molecules. Characterization of the polarity and water distribution profiles in membrane–water interfaces is thus an important issue, and a variety of techniques have been used for this purpose.[2−5]

Reverse micelles (RMs), which form microemulsions in the nanometer range,[6] represent an attractive experimental model of the membrane hydration because their water content can be easily experimentally controlled and thus are frequently used as mimics of the membrane–water interface.[6,7] These nano-objects consist of water-containing assemblies of surfactant molecules with the polar head groups pointing toward an internal aqueous space and the hydrocarbon tails projecting into the surrounding apolar solvent. These entities are able to contain a limited number of water molecules (typically from less than 100 up to several thousand), referred to as the water pool.[8−10] Their water content, defined as $w_0$ (the water to surfactant molar ratio), controls their size,[11] the surfactant polar group packing,[12] their internal fluidity,[11] the water mobility,[9,10,13] and the proton-transfer efficiency.[14] They can incorporate molecules such as peptides, proteins, or nucleic acids.[8,15] This makes it possible to study the conformation and dynamics of these molecules in confined water using a variety of techniques.[16−19] The functional interplay between water and enzymatic functions can also be studied in these microreactors to elucidate the relationships between solvent dynamics and enzymatic kinetics, as well as stability and structure.[20] It has been recently demonstrated that the incorporation of large proteins into RMs in low-viscosity fluids can be used to make such proteins amenable to structural determination by NMR spectroscopy.[21]

Fluorescence spectroscopy has been widely used to study the hydration status and dynamics within membranes and micelles.[13,22−27] This is because the fluorescence emission displays a high sensitivity to polarity in a large set of available probes (polarity-dependent fluorescence Stokes shift). This sensitivity is due to general and specific solvent effects. The reaction field response of the solvent to the change (generally an increase) in the dipole moment of the excited state with respect to that of the ground state stabilizes the excited state. The excited state then fluoresces at lower energy (longer wavelength), leading to a solvent-induced red shift.[28] Specific H-bonding interactions, particularly with hydration water, can also contribute to these spectral shifts. Translation of polarity in terms of water content is highly desirable in membrane studies

**Received:** September 29, 2011
**Revised:** December 15, 2011
**Published:** January 10, 2012





dx.doi.org/10.1021/jp209419y | *J. Phys. Chem. B* 2012, 116, 1687–1699

because hydration plays a prominent role in many of the processes that occur in biological membranes.

This can be performed by using the series of *n*-(9-anthroyloxy) stearic acid (*n*-AS) bearing the fluorescent 9-anthroyloxy group branched by an ester bond at different carbon positions along the stearic chain ($n$ = 2, 3, 6, 7, 9, 10, and 12). This series of probes, originally designed for membrane studies by Waggoner and Stryer,[29] has been shown to insert into lipid bilayers with their acyl chain approximately aligned perpendicular to the membrane plane or radially oriented in surfactant micelles.[30−34] In RMs, they are most likely oriented inside of the surfactant domain with their carboxylic group located in the AOT sulfonate region and their acyl chain projecting toward the organic solvent. These probes have been widely used to quantify mobility and order parameter gradients across lipid bilayers at graded depths, as well as to analyze the effects of acyl chain unsaturation and the influence of sterols.[31,35−40] Moreover, in contrast to the parent molecule anthracene,[41] 9-anthroate displays solvatochromic properties arising from the enhancement of the excited-state dipole moment relative to that of the ground state.[42] This is a result of the rotation of the carboxyl group with respect to the anthracene ring.[43] These solvatochromic properties have been used to study the existence of polarity gradients across both model and biological membranes[32,44,45] and also in detergent micelles.[33,46] The observed fluorescence Stokes shift of the *n*-anthroyloxy probes is however not only due to the solvent but also to the intrinsic excited-state reaction (rotation of the carboxyl group mentioned above), which complicates their use to explore the membrane polarity profiles.[42,43,47,48] It is therefore necessary to delineate the two relaxation processes to study the energetics and dynamics of the interaction with the solvent. Moreover, the 9-anthroate exhibits a strong susceptibility to quenching by water.[42,49] The value of the water quenching rate constant was estimated in water−dioxane mixtures[49,50] and has been used to quantify the amount of water present in detergent micelles.[50]

However, in the course of our studies with *n*-AS, we observed that the value of the water quenching rate constant was dependent on the cosolvent used. Because the quenching mechanism involves only H-donor solvents,[49,50] we re-examined the water fluorescence quenching rate constant value of the 9-anthroyloxy moiety by using the Kamlet−Taft acidity scale.[51] We used this value to evaluate the water penetration gradient through RMs of AOT/water in iso-octane. We further delineated the intra- and intermolecular contributions to the time-dependent fluorescence spectral shifts (TDFSSs) to study the interfacial water relaxation kinetics through these membrane mimics by comparing the TDFSSs measured in the absence ($w_0$ = 0) and presence ($w_0$ = 31) of water. However, water can not only be a H-bond donor/acceptor but can also undergo dipolar interactions. The water-induced TDFSS is thus the combination of these two effects. In an attempt to evaluate the influence of the dipolar interactions only, we also performed experiments in AOT/DMF RMs,[52] DMF being a polar nonprotic solvent.

## EXPERIMENTAL METHODS

**Chemicals.** Sodium bis(2-ethylhexyl)sulfosuccinate (Aerosol OT, AOT) was purchased from Sigma and used as supplied. Solvents were of the highest grade commercially available. The white oils Primol 352 and Marcol 52 were kind gifts from ESSO S. A. F. (Notre-Dame de Gravenchon, France). *n*-AS probes were purchased from Molecular Probes (Eugene, OR).

**Preparation of AOT/RMs in Iso-octane.** They were prepared at room temperature as previously described.[7,13,16] Briefly, a stock solution of 0.1 M AOT in iso-octane was prepared, and the desired volume of Milli-Q (Millipore)-purified water (water/surfactant molar ratio, $w_0$, varied from 0 to 31) or DMF ($w_{DMF}$ = 3) was added. The sample was shaken until it became clear. The RM solution (3 mL) was labeled by adding 2.5 μL of a ∼1 mg/mL THF solution of *n*-AS.

**Steady-State Fluorescence Measurements.** Corrected polarized fluorescence emission spectra were recorded with a Cary Eclipse spectrofluorimeter with a slit width of 5 nm for both excitation and emission.

**Time-Resolved Fluorescence Measurements.** Fluorescence intensity and anisotropy decays were obtained from the polarized $I_{vv}(t)$ and $I_{vh}(t)$ components measured by the time-correlated single-photon counting technique as previously described,[13] except that a diode laser (LDH 370 from Picoquant, Berlin-Adlershof, Germany; maximal emission at 375 nm) operating at 10 MHz was used as an excitation source. Fluorescence photons were detected by either a Hamamatsu microchannel plate (model R3809U-02) or a Hamamatsu fast photomultiplier (model R3235-01). The emission wavelength was selected with a Jobin-Yvon H10 monochromator (bandwidth = 8 nm). $I_{vv}(t)$ and $I_{vh}(t)$ were stored in separated 2K memories of a plug-in multichannel analyzer card (Canberra, France) in a microcomputer, which also controlled automatically the data sampling. This collection was performed by alternately measuring the instrumental response function (IRF) with the scattering of a glycogen solution for 30 s at the emission wavelength and then the parallel and perpendicular components of polarized fluorescence decay for 90 s. The full width at half-maximum (fwhm) of the IRF was ∼200 ps. Analyses of fluorescence intensity decay, $I(t)$, reconstructed from the parallel $I_{vv}(t)$ and perpendicular $I_{vh}(t)$ polarized components, as sums of exponentials, were performed by the maximum entropy method (MEM),[53] as previously described.[54] The software MEMSYS 5 can handle a 150-dimensioned vector, with no a priori assumption concerning the amplitude sign, if required. The latter option was used when exclusively positive amplitudes provided poor results in terms of $\chi$-square values and distribution of the deviation function of the weighted residuals.[13,55]

A classical anisotropy model, in which each lifetime may be coupled to any rotational correlation time, was used to resolve the polarized fluorescence decays.[56] Calculations were performed with a set of 100 independent variables (equally spaced on a logarithmic scale). The programs, including the MEMSYS 5 subroutines (MEDC Ltd., Cambridge, U.K.), were written in double-precision FORTRAN 77.

**Time-Resolved Emission Spectra (TRES) Collection and Analysis.** *n*-AS TRES were reconstructed in each set of experimental conditions from individual decays as a function of emission wavelength from 390 to 550 nm (bandwidth = 5 nm) with 5 nm increments. The MEM program was used to fit individual curves, using the negative amplitude option. At each wavelength, the integral of each fluorescence decay curve was normalized using the corresponding steady-state intensity value. As we collected the vertical and horizontal fluorescence intensity decay components and accounted for the $\beta$ correction factor, the calculated values for impulse fluorescence intensity ($I_{vv}(t) + 2\beta I_{vh}(t)$) and steady-state intensity ($I_{vv} + 2\beta I_{vh}$) were de facto corrected for the difference in transmission of the polarized light components by the optics. We used ∼25 ps


dx.doi.org/10.1021/jp209419y | J. Phys. Chem. B 2012, 116, 1687−1699

steps for spectral shift construction. For a quantitative description of the spectral shift, frequency maxima were used. The time-resolved fluorescence spectra were analytically described using a log-normal function (a skewed Gaussian equation) of the following form[57]

$$I(\nu) = I_m \exp\{-(\ln 2/\ln^2 \rho)\ln^2[(a - \nu)/(a - \nu_m)]\}$$
$$(\text{at } \nu < a)$$
$$I(\nu) = 0 \qquad (\text{at } \nu \geq a)$$

Here, $I_m = I(\nu_m)$ is the maximal fluorescence intensity; $\nu_m$ is the wavenumber of the band maximum (peak); $\rho = (\nu_m - \nu_-)/(\nu_+ - \nu_m)$ is the band asymmetry parameter; $\nu_+$ and $\nu_-$ are the wavenumber positions of left and right half-maximal amplitudes; $a$ is a function the limiting point, $a = \nu_m + \text{fwhm}\ \rho/(\rho^2 - 1)$; and the bandwidth fwhm $= \nu_+ - \nu_-$. Time-resolved spectra were then area-normalized.[58]

**Molecular Modeling and Simulation of the 3-, 7, and 12-AS in AOT–Water RMs in Iso-octane.** The Hyperchem software (Hypercube Inc., Florida) was used to build AOT, *n*-AS, and iso-octane molecules. The preparation of the starting RM followed a protocol identical to that described in Abel et al.[59] A spherical drop of 384 water molecules was selected from a cubic water box after a molecular dynamics (MD) simulation of 40 ps. Then, 64 of the 384 water molecules were randomly and manually replaced by 64 $Na^+$ counterions, and 64 AOT molecules were placed by hand on the above-described sphere, their tails pointing toward the exterior. A 56 Å sized cubic box was filled with iso-octane. A spherical drop of iso-octane equivalent in size with the RM containing water was removed from that box and replaced by the RM containing 384 − 64 = 320 $H_2O$, 64 AOT, and 64 $Na^+$ counterion molecules. Thus, the water content of the simulated micelle corresponds to a $w_0$ value of 5, surrounded by 486 iso-octane molecules in a 56 Å sized cubic box. That box was copied three times, and the *n*-AS ($n$ = 3, 7, and 12) was separately incorporated into each of them. As described in Abel et al.,[59] the equilibration of the system proceeded in two steps, (i) relaxation of iso-octane at 500 K over 100 ps with the frozen RM and (ii) the whole system being frozen at 0 K and then heated at 300 K over 200 ps. All modeling procedures, including energy minimization and MD, were performed using the software Hyperchem 8.0. Energy calculations were carried out using the BIO+ force field, an implementation of the CHARMM force field.[60] Dynamic simulation was performed using a time step of 2.5 fs at a temperature of 300 K, after the equilibration process described above. Snapshots were collected each 100 steps.

## RESULTS

**Quenching of the 9-Anthroyloxy Moiety by Water.** The excited-state lifetime of methyl 9-anthroate is decreased in protic solvents, especially in water–solvent mixtures.[49] The quenching mechanism selectively involved the H-bond formation between a water molecule and the carbonyl of the methyl ester bond of the photoexcited fluorophore.[49] Such a selective mechanism opened the possibility to use this chromophore for quantitative water detection in various media.[61−63] However, for this purpose, the bimolecular quenching constant value for water ($k_{H_2O}$) has to be determined. This has been performed using excited-state lifetime measurements in dioxane–water mixtures, which gave $k_{H_2O}$ values of $10^7$ $M^{-1}$ $s^{-1}$ for 9-anthroate[49] and 5.5 × $10^6$ $M^{-1}$ $s^{-1}$ for *n*-AS,[50] calculated from the slopes of Stern–Volmer plots

$$(\tau_0/\tau) - 1 = k_{H_2O}\tau_0[H_2O]$$

where $\tau_0$ is the excited-state lifetime in the absence of water and $\tau$ is the excited-state lifetime at a particular water concentration $[H_2O]$. Using this method, we found that $k_{H_2O}$ strongly depended on the nature of the water–cosolvent mixture used (Figure 1). The $k_{H_2O}$ values obtained from the excited-state

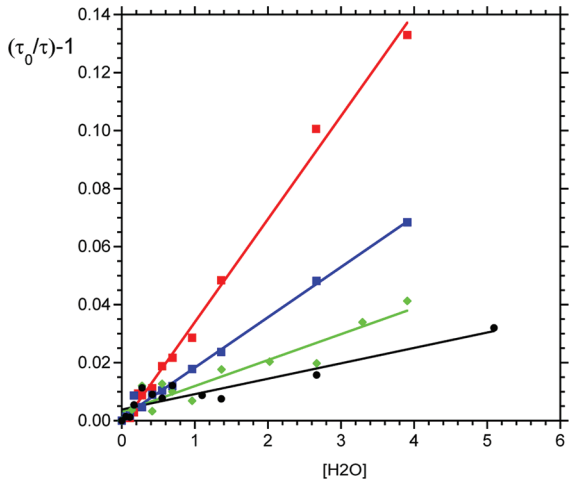


**Figure 1.** Stern–Volmer plots of $(\tau_0/\tau) - 1 = k_{H_2O}\tau_0[H_2O]$ for 12-AS quenching by water in different solvents. $\tau_0$ is the excited-state lifetime in the absence of water, $\tau$ is the excited-state lifetime in the presence of a certain concentration $[H_2O]$ of water, and $k_{H_2O}$ is the water quenching constant. Dioxane (red trace); DMSO (blue trace); DMF (green trace); THF (black trace).

lifetime measured close to the 12-AS emission maxima were 3.4 × $10^6$ $M^{-1}$ $s^{-1}$ in dioxane, 1.7 × $10^6$ $M^{-1}$ $s^{-1}$ in DMSO, 0.9 × $10^6$ $M^{-1}$ $s^{-1}$ in DMF, and 0.5 × $10^6$ $M^{-1}$ $s^{-1}$ in THF. These large differences might be due to the nonideality of these mixed water/organic solvents and the preferential solvation of the fluorophore.[61,64] Furthermore, none of these $k_{H_2O}$ values allow us to compute a lifetime value of ∼300–500 ps for 9-anthroate[42] (estimated from quantum yield measurements) and 300 ps reported for 4-(9-anthroyloxy) butanoic acid in water.[63]

To obtain a quenching constant value independent from the cosolvents, we therefore tried another approach. We used the Kamlet–Taft empirical description of solvent effects on reactivity by the linear free-energy relationship,[51] which is general enough to be applied to almost any type of reaction

$$\log k = s\pi^* + a\alpha + b\beta$$

where $\pi^*$ is a measure of solvent polarity, $\alpha$ and $\beta$ refer to H-bond acidity and basicity, respectively, and $s$, $a$, and $b$ are regression coefficients measuring the susceptibility of the solvent-dependent solute property (here, the excited-state lifetime) to the respective solvent parameter. Because the quenching mechanism of the 9-anthroyloxy group exclusively involves the H-bond acidity of the solvent,[49] only the acidity parameter $\alpha$ was considered. We observed that the variations of the single excited-state lifetime of 3- and 12-AS, measured in alcoholic neat solvents close to the fluorescence emission


dx.doi.org/10.1021/jp209419y | J. Phys. Chem. B 2012, 116, 1687–1699

**Table 1. Excited-State Lifetime Values of 3-AS and 12-AS in Apolar, Polar Nonprotic, And Polar Protic Neat Solvents at 20°C**

| solvent | 3-AS $\tau$ (ns) | 12-AS $\tau$ (ns) | viscosity (cP) | $\alpha_{KT}$[a] |
|---|---|---|---|---|
| Primol | 11.2 | 12.0 | 180 | |
| Marcol | 10.7 | 11.2 | 11 | |
| cyclohexane | 8.3 | 8.2 | 1.03 | |
| iso-octane | 8.5 | 7.8 | 0.55 | |
| *n*-octane | 8.7 | 7.9 | 0.55 | |
| DMSO | 11.1 | 10.4 | 2.14 | |
| dioxane | 11.3 | 10.5 | 1.13 | |
| DMF | 10.5 | 10.3 | 0.92 | |
| THF | 9.4 | 9.1 | 0.55 | |
| propionitrile | 8.3 | 7.9 | 0.44 | |
| cyclohexanol | 8.5 | 8.0 | 41[b] | 0.66 |
| 1-hexanol | 7.3 | 6.9 | 6 | 0.65 |
| *t*-butanol | 6.7 | 6.4 | 3.3 | 0.68 |
| *i*-butanol | 4.8 | 4.7 | 6.68 | 0.69 |
| 1-butanol | 5.8 | 5.3 | 2.98 | 0.71 |
| 2-propanol | 4.8 | 4.7 | 2.50 | 0.76 |
| 1-propanol | 4.4 | 4.3 | 2.30 | 0.78 |
| ethanol | 3.6 | 3.4 | 1.20 | 0.83 |
| methanol | 2.2 | 1.9 | 0.59 | 0.93 |

[a] $\alpha_{KT}$ represents the solvent acidity parameters.[51,74,92] [b] At 25 °C.

maximum (Table 1) correlated strongly with this acidity parameter $\alpha$ (Figure 2). The representation allowed us to

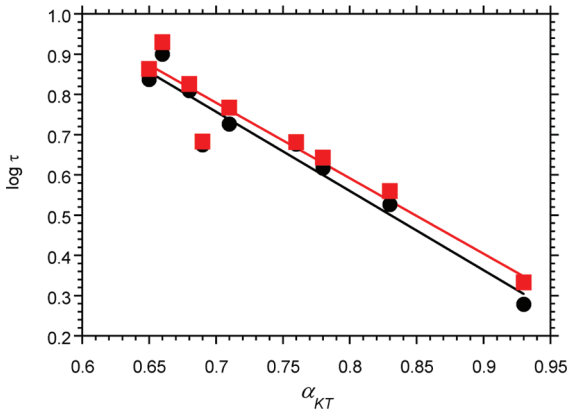


**Figure 2.** Variation of the excited-state lifetime as a function of the 9-anthroyloxy position with the acidity scale $\alpha_{KT}$ of protic solvents. 12-AS (black trace); 3-AS (red trace).

determine an excited-state lifetime value for 3- and 12-AS in water of ~730 ps, close to that in the literature.[42,63] Computation of the $k_{H_2O}$ value also requires measurements of $\tau_0$, the excited-state lifetime value in nonquencher media like iso-octane, cyclohexane, and viscous oils (Marcol 52 and Primol 352). Slight variations of the single excited-state lifetimes measured at the maximum of the emission spectrum in these solvents were observed with their viscosity (Table 1). As a reference, we used the average lifetime value for 3- and 12-AS in cyclohexane ($\tau$ = 8.2 ns), a solvent similar in viscosity to water at 20 °C. We then obtained a $k_{H_2O}$ value of 2.3 × $10^7$ $M^{-1}$ $s^{-1}$ that we further used to estimate the water concentration in RMs. Using either the longer-lifetime values measured in the highest-viscosity solvent Primol 352 or the shorter one in the lowest-viscosity solvent iso-octane did not significantly alter the calculated $k_{H_2O}$ value (2.4 × $10^7$ or 2.2 × $10^7$ $M^{-1}$ $s^{-1}$, respectively).

**Intramolecular Excited-State Relaxation versus Solvent-Induced Relaxation in 12-AS.** *Measurements in Hydrocarbon Apolar Solvents.* In high-viscosity hydrocarbon apolar solvent (white oil Primol 352), fluorescence intensity decay measurements of 12-AS, taken as a representative example of the *n*-AS probes, were recorded as a function of emission wavelength. On the blue edge of the fluorescence emission spectrum, a fast decay followed by a long one is observed (Figure 3, upper panel). MEM analysis of this decay showed emission heterogeneity (Figure 3 upper panel, left inset). On the red edge of the emission spectrum, fast fluorescence buildup was observed followed by a slow emission component (Figure 3, upper panel). MEM analysis reported a short time component (~1 ns) affected by the negative amplitude and a long lifetime (~10 ns) of the same order of magnitude as that observed in the blue-edge region (Figure 3, upper panel, right inset). Similar effects were observed for other *n*-AS derivatives and also in Marcol 52 (data not shown). These time-dependent features characterize a spectral shift occurring in the time range of the excited-state lifetime and originating from the well-known excited-state internal relaxation of the 9-anthroyloxy moiety.[47,48] The anthracene ring rotates from a perpendicular conformation with respect to the carboxylic group of the ester bond in the ground state to a major "coplanar" one in the excited state.[42,48,65] However, the heterogeneity of the lifetime distribution on the blue edge suggests an initial distribution of excited-state conformations.

The kinetic and energetic parameters of the intramolecular excited-state relaxation in these two highly viscous hydrocarbon solvents (Primol 352 and Marcol 52) can be estimated by time-resolved emission spectra (TRES) analysis.[66] The TDFSS kinetics was modeled by two exponentials and a constant term, each transient spectra being modeled by a Gaussian log-normal function;[13,57] two Gaussians provided no better fit. In the highest viscous solvent (Primol 352), the initial spectrum peaked at $\lambda_0$ = 434 nm (Table 2), a value shifted by ~14 nm with respect to that measured in glass solvents (420 nm).[65] In Marcol 52, which exhibited a lower viscosity than Primol 352, the initial spectrum peeked at a more red-shifted $\lambda_0$ = 443 nm (Table 2). The maximum emission wavelength at infinite time $\lambda_\infty$, which describes the energy state of the relaxed coplanar charge transfer (CT), leveled up at ~454−455 nm for both solvents (Table 2). This corresponds to the maxima of the steady-state fluorescence spectrum in each solvent. The multiexponential kinetics of the TDFSS (Figure 4, upper panel, inset) occurred on subnanosecond and tens of nanosecond time scales (Table 2). We did not observe any isoemissive point in the time-resolved area normalized emission spectra TRANES,[58] in disagreement with a simple two-state process (Figure 4, upper panel). MD simulations[65] and excited-state lifetime measurements on the blue edge of the fluorescence emission spectrum (Figure 3, upper panel, left inset) suggest the existence of multiple excited-state configurations evolving with time. The final excited-state configuration is characterized by a single excited-state lifetime on the red edge of the fluorescence spectrum (Figure 3, upper panel, right inset). The excited-state stabilization energy due to the intramolecular rotational relaxation was ~5.1 kcal $M^{-1}$. This corresponds to a spectral shift of ~1800 $cm^{-1}$ (35 nm) calculated from the estimated value in glass solvents.[65]


dx.doi.org/10.1021/jp209419y | J. Phys. Chem. B 2012, 116, 1687−1699

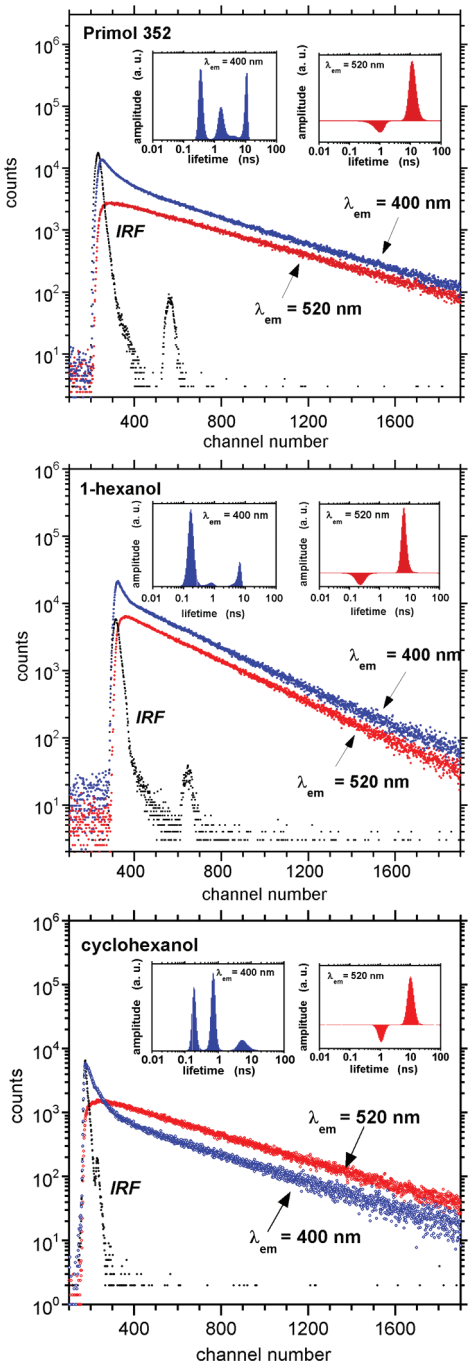


**Figure 3.** Fluorescence intensity decays of 12-AS in neat solvents. (Upper panel) Primol 352. Blue curves: Fluorescence intensity decay and lifetime distribution recovered by MEM (left inset) at an emission wavelength of 400 nm; red curves: fluorescence intensity decay and lifetime distribution recovered by MEM (right inset) at an emission wavelength of 520 nm. (Middle panel) 1-Hexanol. Blue curves: fluorescence intensity decay and lifetime distribution recovered by MEM (left inset) at an emission wavelength of 400 nm; red curves: fluorescence intensity decay and lifetime distribution recovered by MEM (right inset) at an emission wavelength of 520 nm. (Lower panel) Cyclohexanol. Blue curves: fluorescence intensity decay and lifetime distribution recovered by MEM (left inset) at an emission wavelength of 400 nm; red curves: fluorescence intensity decay and lifetime distribution recovered by MEM (right inset) at an emission wavelength of 520 nm. IRF: instrumental response function. Time resolution: 25 ps/cl.

*Measurements in Polar Protic Neat Solvents.* The steady-state emission spectra of *n*-AS in protic polar solvents were red-shifted compared to those in apolar ones. Ethanol and methanol displayed the largest red shift (not shown). No fluorescence buildup could be observed in fluorescence decay measurements on the red edge of the fluorescence emission spectrum for these alcohols of low viscosity; both the intramolecular and the solvent relaxation processes are likely to be very fast in these solvents (data not shown). Increasing the viscosity of the alcohols allowed detection of fast fluorescence decay for *n*-AS on the blue edge of the fluorescence emission spectra and a fluorescence buildup on the red edge, as exemplified for 12-AS in Figure 3 (middle panel for 1-hexanol and lower panel for cyclohexanol). This is likely due to intramolecular and/or solvent relaxation processes. Theses initial fast processes are followed by the emission decay of the relaxed excited state. MEM analysis of the decays on the blue edge of 1-hexanol showed a lifetime distribution simply characterized by two peaks of positive amplitude (Figure 3, middle panel, left inset). On the red edge, the distributed lifetime showed positive and negative amplitudes, for which the respective barycenters correspond to those observed on the blue edge (~150−200 ps, fluorescence lifetime = 6.9 ns) (Figure 3, middle panel, right inset). Such a similarity of the fast decay times in the extreme regions of the fluorescence emission spectra was noticed when the relaxational component was much faster than the fluorescence lifetime.[67] The long-lived emission is characterized by a sharp lifetime peak whatever the emission wavelength (not shown).

The same analysis for cyclohexanol, the polar protic solvent used in this work with a viscosity comparable to that of the viscous hydrocarbon apolar Primol 352, showed more complex features in the spectral blue spectral region with three lifetime populations of positive amplitude (Figure 3, lower panel, left inset). Thus, the emission process likely involved more than two states. On the red edge of the fluorescence spectrum, we observed a single rise time much longer than that in 1-hexanol (~0.9 ns) (Figure 3, lower panel, right inset). This is in accordance with the difference in viscosity of the two alcohols. In this long-wavelength spectral region, the fluorescence decay shows a single excited-state lifetime (~8 ns), indicating homogeneity of the final solvent-relaxed excited state.

In the two alcohols of intermediate viscosity, 1-hexanol (Figure 4, middle panel) and isobutanol (not shown), TRANES displayed an isoemissive point at ~460 nm, which was indicative of a two-state relaxation process, consistent with the fluorescence decay characteristics (Figure 4, middle panel). The maximum emission wavelengths at infinite time ($\lambda_\infty$) of the TDFSSs in these two alcohols were identical (Table 2). Moreover, these values are similar to the maximum emission wavelengths of the steady-state fluorescence spectra in the alcohols of lowest viscosity (methanol: 474 nm; ethanol: 471 nm).

In the high-viscosity alcohol cyclohexanol, TRANES did not exhibit any isoemissive point (Figure 4, lower panel), but instead, the spectral shift appeared to be continuous over subnano- and nanosecond time scales (Table 2). TDFSS is characterized by an initial maximum emission wavelength of $\lambda_0$ = 448 nm, which is close to the $\lambda_\infty$ value measured in apolar viscous solvents (Table 2), characteristic of the coplanar excited-state conformation. The intramolecular relaxation rate was therefore strongly increased and could not be measured with our instrumentation in this protic solvent, despite its high viscosity. The maximum emission wavelength value at infinite time ($\lambda_\infty$) was red-shifted by ~20 nm as compared to that in apolar solvents (Table 2).


dx.doi.org/10.1021/jp209419y | J. Phys. Chem. B 2012, 116, 1687−1699

**Table 2. Parameters of the TDFSS of 12-AS in Neat Solvents**[a]

| solvents | $\bar{\nu}_0$ ($cm^{-1}$) | $\lambda_0$ (nm) | $\bar{\nu}_\infty$ ($cm^{-1}$) | $\lambda_\infty$ (nm) | $\Delta\bar{\nu}$ ($cm^{-1}$)[b] | $\Delta\lambda$ (nm)[b] | $\tau_{r1}$ (ns) | $\Delta\bar{\nu}_1/\Delta\bar{\nu}$ | $\tau_{r2}$ (ns) | $\Delta\bar{\nu}_2/\Delta\bar{\nu}$ |
|---|---|---|---|---|---|---|---|---|---|---|
| Primol 352 | 23038 | 434 | 22043 | 454 | 995 | 20 | 0.8 | 0.67 | 14 | 0.33 |
| Marcol 52 | 22564 | 443 | 21984 | 455 | 580 | 12 | 0.4 | 0.45 | 16 | 0.55 |
| Cyclohexanol | 22307 | 448 | 21097 | 474 | 1196 | 26 | 0.4 | 0.51 | 1.4 | 0.49 |
| 1-Hexanol | 22075 | 453 | 21151 | 473 | 924 | 20 | 0.2 | 0.56 | 0.9 | 0.44 |
| Isobutanol | 21392 | 467 | 21040 | 475 | 352 | 8 | 0.1 | 0.87 | 1.1 | 0.13 |

[a]The TDFSSs were fitted by the equation $\bar{\nu} = \Delta\bar{\nu}_1 \exp(-t/\tau_{r1}) + \Delta\bar{\nu}_2 \exp(-t/\tau_{r2}) + \bar{\nu}_\infty$. [b]$\Delta\bar{\nu} = [\bar{\nu}_0 - \bar{\nu}_\infty]$; $\Delta\lambda = [\lambda_\infty - \lambda_0]$.

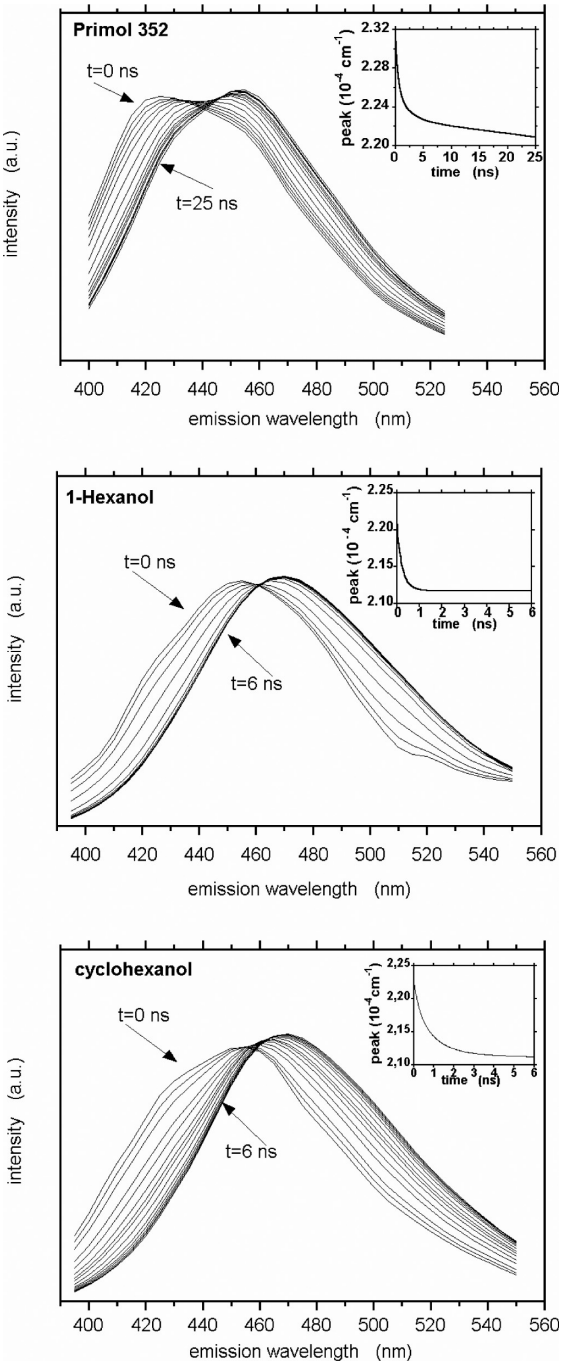


**Figure 4.** TRANES of 12-AS in neat solvents. (Upper panel) Primol 352. (Middle panel) 1-Hexanol. (Lower panel) Cyclohexanol. (Insets) Variation of the transient emission spectral peak in each solvent.

On average, the excited-state stabilization energy ($\Delta E \approx 2.5$ kcal.$M^{-1}$) in polar protic solvents might contain two terms originating from general dipolar interactions and specific H-bonds. To estimate the respective contributions of these two terms, we performed measurements in polar aprotic solvents.

*Measurements in Polar Aprotic Neat Solvents.* The steady-state emission spectra of *n*-AS in polar aprotic solvents such as DMF and DMSO were red-shifted by ~10−13 nm ($\lambda_{max}$ = 465−468 nm for 12-AS as an example) with respect to the emission spectra in hydrocarbon solvents. Both the intramolecular and solvent relaxation processes were extremely fast in these low-viscosity solvents, and no TDFSS could be recorded with our instrument. Considering the steady-state data, the stabilization energy of the excited state by the general dipolar solvent effect was ~550 $cm^{-1}$ ($\Delta E \approx 1.6$ kcal.$M^{-1}$). Considering the stabilization energy calculated in polar protic solvents (preceding paragraph), the H-bond interaction energy therefore can be estimated to be ~1 kcal $M^{-1}$.

**Water Distribution Profile in AOT/Water RMs.** The fluorescence intensity decays measured at the maximum of the emission spectrum of the 9-anthroyloxy moiety for each *n*-AS derivative in RMs displayed one major excited-state lifetime population whatever the $w_0$ (Figure 5, illustration for 2-AS, upper panel inset for $w_0$ = 0 and 31). In the absence of water ($w_0$ = 0), the excited-state lifetime value did not vary by more than 6% (mean = 9.3 ± 0.6 ns) for the different *n*-AS derivatives. Upon increasing the water content, the excited-state lifetime progressively shortened (Figure 5, middle panel). The dynamic quenching efficiency by water progressively decreased from the shallowest (2- and 3-AS) to the intermediates probes (6-, 7-, and 9-AS), while very small or no quenching occurred for 10- and 12-AS, respectively. The local water concentration in the vicinity of the 9-anthroyloxy carbonyl group could then be estimated using the expression[49]

$$[H_2O] = \left(\frac{1}{\tau} - \frac{1}{\tau_0}\right) \times \frac{1}{k_{H_2O}}$$

where $\tau_0$ is the excited-state lifetime of the *n*-AS under consideration at $w_0$ = 0. The water concentration (calculated from $k_{H_2O}$) progressively decreased with the labeled depth (Figure 5, lower panel). At high $w_0$ values, the local water concentration was estimated to be ~9 M around the shallowest 2- and 3-AS positions and to ≤2 M around the intermediate ones (7- and 9-AS). No water was detected by 12-AS. At lower $w_0$, the local water concentration decreased for each position. At $w_0$ = 3.5 and 7, we observed that the trend of the water profiles obtained in our measurements was similar to that in recent MD calculations.[59,68]

**Water-Induced Spectral Relaxation of *n*-AS in AOT/Water RMs: Steady-State Fluorescence Emission Spectra and TRES Measurements.** The steady-state fluorescence emission spectra of the *n*-AS probes incorporated in RMs peaked at ~455−457 nm in the absence of trapped water


dx.doi.org/10.1021/jp209419y | J. Phys. Chem. B 2012, 116, 1687−1699

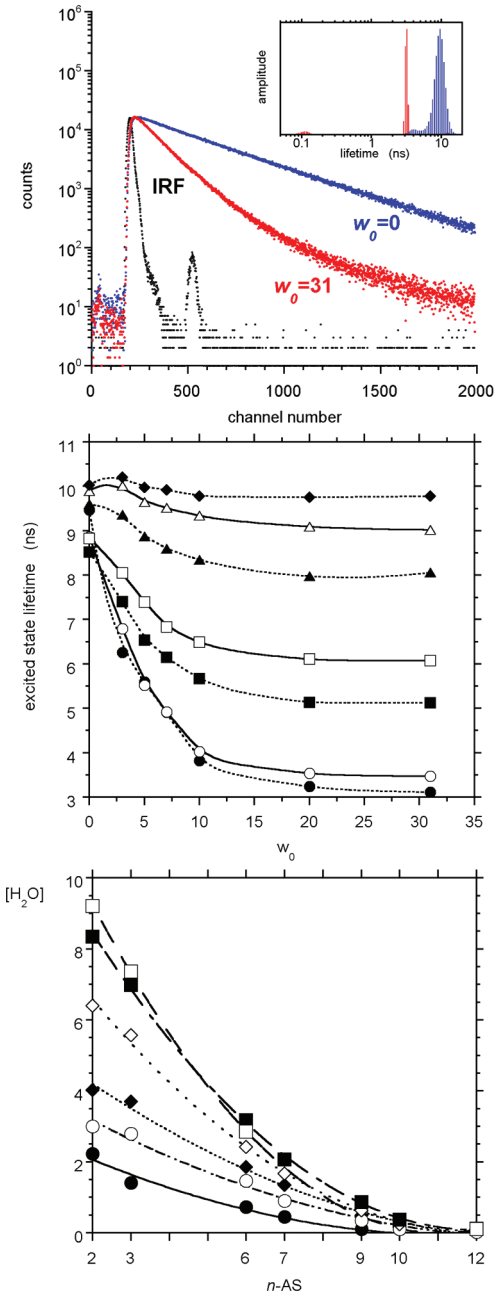


**Figure 5.** Fluorescence intensity decays of 2-AS in RMs and the water concentration gradient in RMs as a function of the 9-anthroyloxy position and $w_0$. (Upper panel) Fluorescence intensity decay of 2-AS in RMs. Blue trace: $w_0$ = 0 and emission wavelength = 465 nm; red trace: $w_0$ = 31 and emission wavelength = 480 nm. IRF: instrumental response function. Time resolution: 25 ps/cl. (Inset) Excited-state lifetime distribution recovered by MEM. Blue trace: $w_0$ = 0 and emission wavelength = 465 nm; red trace: at $w_0$ = 31 and emission wavelength = 480 nm. (Middle panel) Variations of the excited-state lifetime value for the series of *n*-AS in RMs as a function of $w_0$. (●) 2-AS; (○) 3-AS; (■) 6-AS; (□) 7-AS; (▲) 9-AS; (Δ) 10-AS; and (♦) 12-AS. (Lower panel) Water concentration gradient in RMs as a function of the 9-anthroyloxy position and $w_0$: (●) 1.8; (○) 5; (♦) 7.7; (Δ) 10.5; (■) 19.3; (□) 31.1.

($w_0$ = 0) (Figure 6), comparable to the values in hydrocarbon solvents. Addition of water induced a red shift of the emission maximum by 10−13 nm for the fluorophore located near the interface with water (2-AS, Figure 6). This shift decreased at

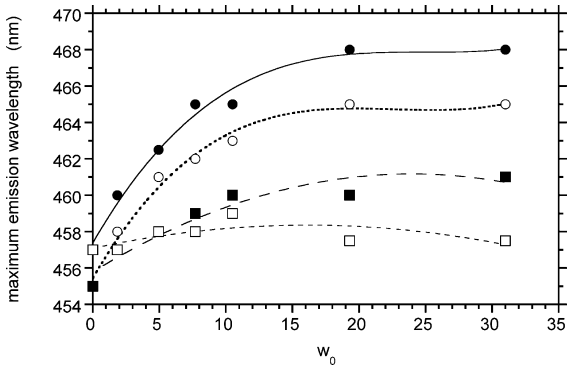


**Figure 6.** Variation of the maximum emission wavelength of the steady-state fluorescence emission spectra of *n*-AS in RMs at different $w_0$: (●) 2-AS; (○) 3-AS; (■) 7-AS; (□) 12-AS.

deeper positions (3- and 7-AS), and no shift at all affected the 12-AS derivative probing the hydrocarbon tail of the surfactant (Figure 6). The dynamics of the spectral shift was then studied by excited-state lifetime and TRES measurements.

In the absence of water ($w_0$ = 0), we observed the signatures of the intramolecular relaxation process on the fluorescence intensity decays measured on the blue and the red edges of the fluorescence emission spectrum, as shown for 3-AS in Figure 7. On the blue edge of the fluorescence emission, we observed multiexponential fast decay kinetics (Figure 7, upper panel, left inset) followed by a long-lived emission (∼9−10 ns). On the red edge of the fluorescence emission, a buildup kinetics characterized the fluorescence decay. It likely corresponds to a multirelaxation process because it was mainly described by two time constants of ∼0.2 and ∼1 ns, which were affected by negative amplitudes (Figure 7, upper panel, right inset). We observed the same two time components as those on the blue edge but associated with positive amplitudes. Such a multiexponential feature of the fluorescence buildup was not observed in neat solvents and may reflect the heterogeneity of the AOT polar head group region. A long-lived lifetime of ∼9 ns characterized the emission of the final coplanar CT relaxed state in an anhydrous environment (Figure 7, upper panel, right inset). TRANES did not evidence any isoemissive point (Figure 7, lower panel), confirming the heterogeneity of excited states at short time that was suggested by the fluorescence decay in the blue spectral region. The maximum emission wavelength at infinite time ($\lambda_\infty$) of the TDFSS reached similar plateau values (455 ± 2 nm) for all *n*-AS (Table 3), similar to the value in hydrocarbon solvents (Table 2). The initial intramolecular relaxation kinetics was extremely fast and not measurable with our instrument because the recorded initial emission spectrum peaked at $\lambda_0$ = 443 nm on average (Table 3). The observable TDFSS was multiphasic on the subnano- and nanosecond time scales. The intramolecular excited-state relaxation was slower in the middle of the surfactant acyl chain region probed by the 6- and 7-AS (i.e., in the branching region of the AOT ethyl chain) than at shallower and deeper positions (Table 3).

In the presence of water, the fluorescence intensity decays (as shown for 3-AS at $w_0$ = 7.7 as an example) exhibited fast decay kinetics and fluorescence buildup on the blue and red edges of the fluorescence emission spectrum, respectively (Figure 8, upper panel). We observed multiexponential buildup kinetics with time components of ∼0.1 and ∼1 ns, which indicated the existence of excited-state relaxation heterogeneity.


dx.doi.org/10.1021/jp209419y | J. Phys. Chem. B 2012, 116, 1687−1699

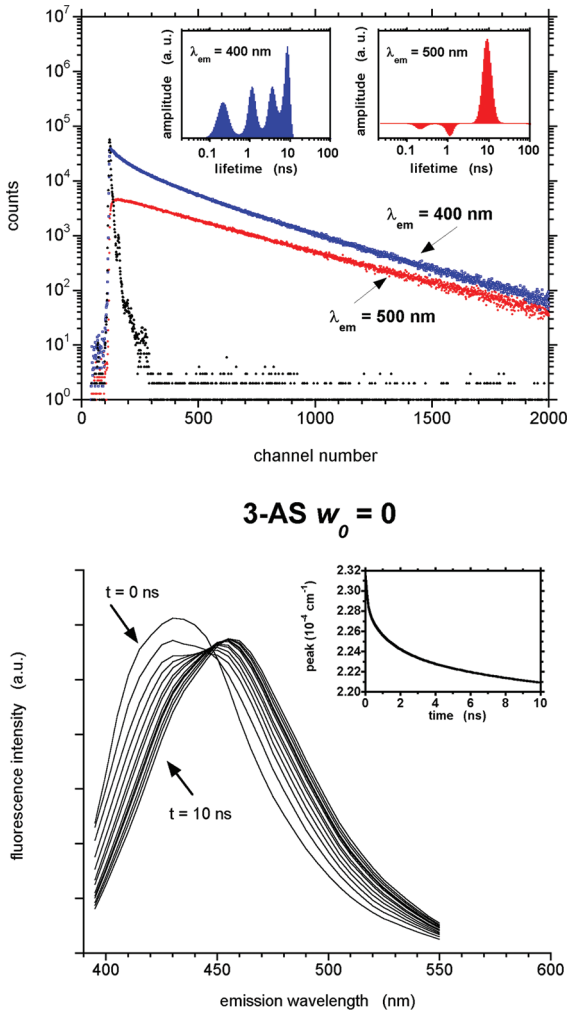


**Figure 7.** Fluorescence intensity decays and TRANES of 3-AS in RMs at $w_0$ = 0. (Upper panel) Fluorescence intensity decay. Blue traces: emission wavelength = 400 nm; (left inset) fluorescence lifetime distribution. Red traces: emission wavelength = 500 nm; (right inset) fluorescence lifetime distribution. Black points: instrumental response function. Time resolution: 25 ps/cl. (Lower panel) TRANES. (Inset) Variation of the transient emission spectral peak in each solvent.

TRANES did not identify any isoemissive point (e.g., Figure 8, lower panel for 3-AS at $w_0$ = 7.7).

On average, over the series of *n*-AS, the TDFSS started at $\lambda_0$ = 451 ± 2 nm (close to the $\lambda_\infty$ value measured in the absence of water, 455 ± 2 nm) (Table 3), which is characteristic of the coplanar state emission. The closer that the fluorophore is to the water interface, the larger the TDFSS at infinite time (479 and 461 nm for 2- and 12-AS, respectively) (Figure 9 and Table 3). For 12-AS, which probed a region devoid of water molecules, as shown by lifetime measurements, a slight shift of only ∼4 nm was observed. The water-induced spectral shift kinetics was multiphasic and could be modeled by a biexponential function in each case with time constants of ∼0.1 and 1−2 ns; a slight slowing down was observed at deeper positions compared with shallow ones (Table 3).

**TRES Measurements in AOT/DMF RMs.** We assumed that the TDFSS observed in AOT/water RMs could be due to H-bond and/or dipolar relaxations. To separate these two mechanisms, we performed TRES measurements with 2-, 3-, 6-, 7-, and 12-AS in AOT/DMF RMs at $w_{DMF}$ = 3 for the sake of comparison with water-containing RMs (at $w_0$ = 31)because the DMF-containing RMs swell much more than those containing water.[27,69] DMF is an aprotic polar solvent bearing a very large dipole moment (3.86 D). The DMF-induced TDFSSs for the shallower probes displayed significantly smaller $\lambda_\infty$ values than those in AOT/water RMs, whereas they were identical for the deepest one 12-AS (Figure 9 and Table 3). This dipolar relaxation process was multiphasic in the subnano- and nanosecond time ranges for all fluorophore positions (Table 3) and was very slowed down compared with that in neat DMF.

**Rotational Dynamics of the *n*-AS in AOT/Water RMs.** To obtain a more complete dynamic description of these nanoobjects, we investigated the rotational motion of the *n*-AS series of probes by time-resolved fluorescence anisotropy decay measurements. These measurements may reflect the dynamics of the surfactant at different depths in the micelles. The fluorescence anisotropy decays (Figure 10, upper panel) followed biexponential behavior (Figure 10, upper panel, inset), as found in many reported cases.[13,70−72] As with other probes such as laurdan,[13] we did not observe Brownian rotational motion of

**Table 3. Parameters of the TDFSS of *n*-AS in AOT/Water and in AOT/DMF RMs in iso-octane[a]**

| sample | $\bar{\nu}_0$ (cm$^{-1}$) | $\lambda_0$ (nm) | $\bar{\nu}_\infty$ (cm$^{-1}$) | $\lambda_\infty$ (nm) | $\lambda_{ss}$ (nm)[c] | $\Delta\bar{\nu}_{solv}$ (cm$^{-1}$)[b] | $\Delta\lambda_{solv}$ (nm)[b] | $\tau_{r1}$ (ns) | $\Delta\bar{\nu}_1/\Delta\bar{\nu}_t$ | $\tau_{r2}$ (ns) | $\Delta\bar{\nu}_2/\Delta\bar{\nu}_t$ |
|---|---|---|---|---|---|---|---|---|---|---|---|
| 2-AS, $w_0$ = 0 | 22534 | 444 | 21930 | 456 | 453 | | | 0.3 | 0.51 | 4.5 | 0.49 |
| 2-AS, $w_0$ = 31 | 22088 | 453 | 20895 | 479 | 464 | 1035 | 23 | 0.2 | 0.48 | 1.2 | 0.52 |
| 3-AS, $w_0$ = 0 | 23126 | 432 | 22059 | 453 | 455 | | | 0.3 | 0.41 | 3.8 | 0.59 |
| 3-AS, $w_0$ = 31 | 22224 | 450 | 21189 | 472 | 465 | 870 | 19 | 0.2 | 0.46 | 1.3 | 0.54 |
| 6-AS, $w_0$ = 0 | 22480 | 445 | 22021 | 454 | 455 | | | 0.7 | 0.36 | 7.3 | 0.64 |
| 6-AS, $w_0$ = 31 | 22061 | 453 | 21450 | 466 | 462 | 571 | 12 | 0.4 | 0.34 | 2.0 | 0.66 |
| 7-AS, $w_0$ = 0 | 22430 | 446 | 21966 | 455 | 455 | | | 0.7 | 0.41 | 7.4 | 0.59 |
| 7-AS, $w_0$ = 31 | 22156 | 451 | 21546 | 464 | 459 | 454 | 10 | 0.4 | 0.38 | 2.5 | 0.62 |
| 12-AS, $w_0$ = 0 | 22329 | 448 | 21874 | 457 | 455 | | | 0.3 | 0.24 | 5.3 | 0.76 |
| 12-AS, $w_0$ = 31 | 22256 | 449 | 21714 | 461 | 458 | 160 | 4 | 0.2 | 0.24 | 2.5 | 0.76 |
| 2-AS, $w_{DMF}$ = 3 | 22203 | 450 | 21474 | 466 | 462 | 456 | 10 | 0.2 | 0.45 | 2.9 | 0.55 |
| 3-AS, $w_{DMF}$ = 3 | 22290 | 449 | 21545 | 464 | 460 | 514 | 11 | 0.2 | 0.58 | 3.4 | 0.42 |
| 6-AS, $w_{DMF}$ = 3 | 22486 | 445 | 21682 | 461 | 460 | 339 | 7 | 0.1 | 0.62 | 2.2 | 0.38 |
| 7-AS, $w_{DMF}$ = 3 | 22435 | 446 | 21669 | 462 | 458 | 297 | 7 | 0.1 | 0.59 | 2.2 | 0.41 |
| 12-AS, $w_{DMF}$ = 3 | 22026 | 454 | 21650 | 462 | 459 | 224 | 5 | 0.4 | 0.40 | 3.4 | 0.60 |

[a]The TDFSSs were fitted by the equation $\bar{\nu}_{(t)} = \Delta\bar{\nu}_1 \exp(-t/\tau_{r1}) + \Delta\bar{\nu}_2 \exp(-t/\tau_{r2}) + \bar{\nu}_\infty$. [b]$\Delta\bar{\nu}_{solv} = [\bar{\nu}_{\infty,w_0=0} - \bar{\nu}_{\infty,w_0 \text{or } w_{DMF}\neq 0}]$; $\Delta\lambda_{solv} = [\lambda_{\infty,w_0 \text{or } w_{DMF}\neq 0} - \lambda_{\infty,w_0=0}]$. [c]Maximum emission wavelength of the steady-state emission spectrum.


dx.doi.org/10.1021/jp209419y | J. Phys. Chem. B 2012, 116, 1687−1699

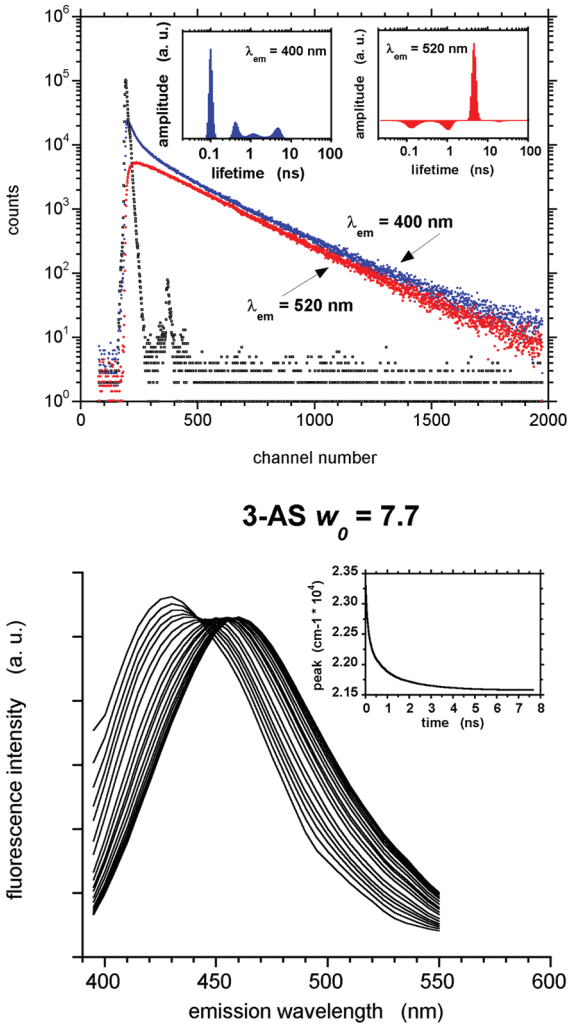


**Figure 8.** Fluorescence intensity decays and TRANES of 3-AS in RMs at $w_0$ = 7.7. (Upper panel) Fluorescence intensity decay. Blue traces: emission wavelength = 400 nm; (left inset) fluorescence lifetime distribution. Red traces: emission wavelength - 520 nm; (right inset) fluorescence lifetime distribution. Black points: instrumental response function. Time resolution: 25 ps/cl. (Lower panel) TRANES. (Inset) Variation of the transient emission spectral peak in each solvent.

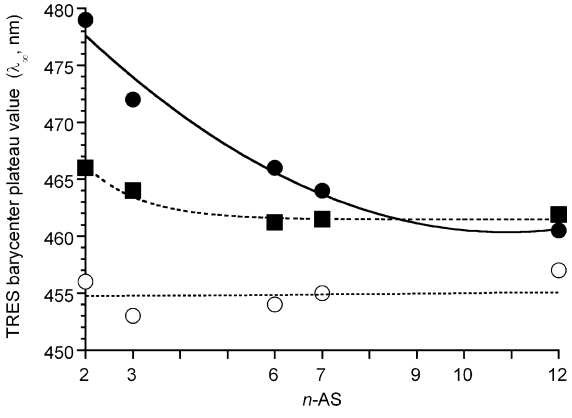


**Figure 9.** Maximum emission wavelength at infinite time ($\lambda_\infty$) as a function of the 9-anthroyloxy position in RMs. (○) AOT/water RMs at $w_0$ = 0; (●) AOT/water RMs at $w_0$ = 31; (ν) AOT/DMF RMs at $w_{DMF}$ = 3.

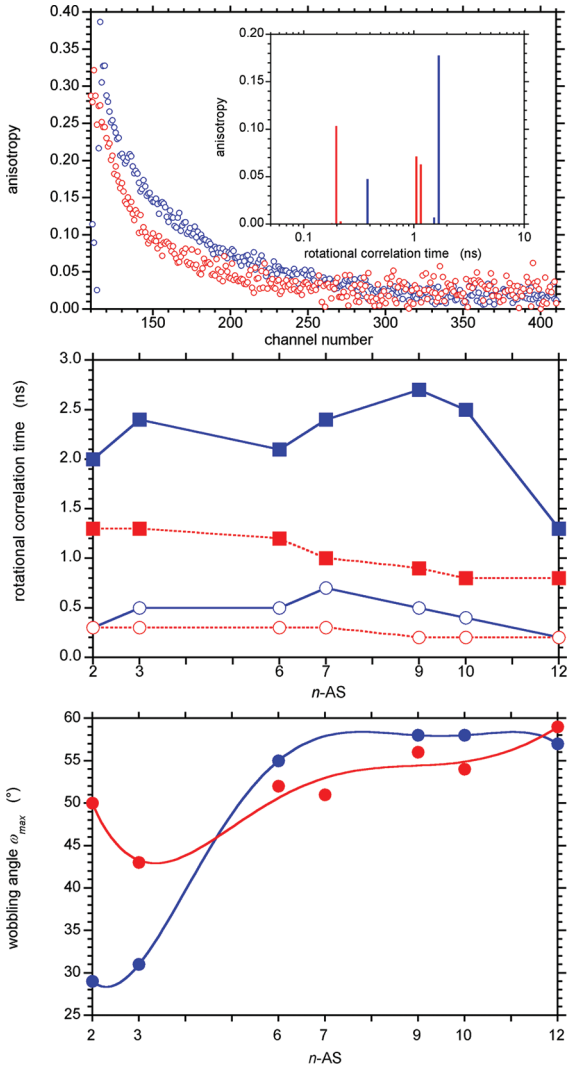


**Figure 10.** Fluorescence anisotropy decays of *n*-AS in AOT/water RMs. (Upper panel) Experimental fluorescence anisotropy decay traces for 3-AS at $w_0$ = 0 (blue trace) and 31 (red trace). Time resolution: 25 ps/cl. (Inset) Respective rotational correlation time distribution recovered by MEM. (Middle panel) Rotational correlation times of *n*-AS at $w_0$ = 0 (blue traces) and 31 (red traces). (Lower panel) Semi-angle of the wobbling-in-cone motion $\omega_{max}$ of *n*-AS at $w_0$ = 0 (blue traces) and 31 (red traces). Its value was calculated from $\beta_2/r_0 = [1/2 \cos \omega_{max}(1 + \cos \omega_{max})]^2$,[89] where $r_0$ = 0.290, the steady-state anisotropy value in vitrified media at 370 nm as excitation wavelength.[36]

the micelle itself except at the lowest $w_0$ (Table 4). This suggests that these two rotational correlation times most likely described the local rotational dynamics of the 9-anthroyloxy group. We previously showed that the 9-anthroyloxy rotational dynamics could be rationalized in terms of in- and out-of-plane rotations.[38−40] The in-plane rotation depended on the acyl chain segmental reorientation motion, whereas the out-of-plane rotation occurred independently around the ester bond at C9 on the anthracene ring. At an excitation wavelength of 370 nm (which we used in the present study), both rotations contributed to the depolarization.[38] It is likely that the subnanosecond rotational correlation time observed in RMs corresponded to the in-plane rotation of the 9-anthroyloxy moiety. This rotation was partially restricted by the local segmental motions of the stearoyl chain encased in the surfactant acyl chain region. In the absence of water ($w_0$ = 0), this rotation was more restricted at


dx.doi.org/10.1021/jp209419y | J. Phys. Chem. B 2012, 116, 1687−1699

Table 4. Fluorescence Anisotropy Decay, $r(t) = \sum_i \beta_i \exp(-t/\theta_i)$, of *n*-AS in RMs[a]

| *n*-AS | $w_0$ | $\beta_1$ | $\beta_2$ | $\theta_1$ (ns) | $\theta_2$ (ns) | $r_{t=0} = \sum \beta_i$ | $\omega_{max}$ (°) |
|---|---|---|---|---|---|---|---|
| 2-AS | 0 | 0.076 ± 0.013 | 0.197 ± 0.019 | 0.3 ± 0.2 | 2.0 ± 0.2 | 0.273 ± 0.020 | 29 ± 3 |
| 3-AS | 0 | 0.050 ± 0.013 | 0.185 ± 0.023 | 0.5 ± 0.2 | 2.4 ± 0.4 | 0.235 ± 0.020 | 31 ± 4 |
| 6-AS | 0 | 0.095 ± 0.013 | 0.058 ± 0.011 | 0.5 ± 0.1 | 2.1 ± 0.1 | 0.153 ± 0.010 | 55 ± 3 |
| 7-AS | 0 | 0.089 ± 0.013 | 0.037 ± 0.006 | 0.7 ± 0.2 | 2.4 ± 0.5 | 0.126 ± 0.010 | 61 ± 3 |
| 9-AS | 0 | 0.093 | 0.049 | 0.5 | 2.7 | 0.144 | 58 |
| 10-AS | 0 | 0.106 ± 0.010 | 0.046 ± 0.007 | 0.4 ± 0.2 | 2.5 ± 0.2 | 0.152 ± 0.010 | 58 ± 3 |
| 12-AS | 0 | 0.049 ± 0.019 | 0.053 ± 0.004 | 0.20 ± 0.03 | 1.3 ± 0.1 | 0.102 ± 0.015 | 57 ± 1 |
| 2-AS | 31 | 0.145 ± 0.037 | 0.080 ± 0.040 | 0.3 ± 0.1 | 1.8 ± 0.8 | 0.225 ± 0.050 | 50 ± 8 |
| 3-AS | 31 | 0.106 ± 0.011 | 0.116 ± 0.013 | 0.3 ± 0.1 | 1.3 ± 0.1 | 0.222 ± 0.010 | 43 ± 2 |
| 6-AS | 31 | 0.090 ± 0.003 | 0.071 ± 0.023 | 0.3 ± 0.2 | 1.2 ± 0.3 | 0.161 ± 0.020 | 52 ± 6 |
| 7-AS | 31 | 0.088 ± 0.024 | 0.071 ± 0.006 | 0.20 ± 0.01 | 1.0 ± 0.1 | 0.159 ± 0.020 | 51 ± 3 |
| 9-AS | 31 | 0.122 | 0.053 | 0.2 | 0.9 | 0.175 | 56 |
| 10-AS | 31 | 0.038 ± 0.020 | 0.057 ± 0.014 | 0.2 ± 0.1 | 0.8 ± 0.2 | 0.095 ± 0.020 | 54 ± 2 |
| 12-AS | 31 | 0.054 ± 0.012 | 0.045 ± 0.002 | 0.20 ± 0.02 | 0.8 ± 0.1 | 0.099 ± 0.010 | 59 ± 1 |

[a]The semi-angle of the wobbling-in-cone motion $\omega_{max}$ was calculated from the equation $\beta_2/r_0 = [1/2 \cos \omega_{max}(1 + \cos \omega_{max})]^2$, where $r_0 = 0.290$ is the steady-state anisotropy value in vitrified media.[38] Mean and standard deviation values from 2−3 measurements are shown.

the polar interface than that at deeper positions, as suggested by lower values of the wobbling-in-cone semiangle $\omega_{max}$ for the 2- and 3-AS compared with those for the other *n*-AS derivatives (Figure 10, lower panel and Table 4). With the addition of water inside of the RMs, this rotational motion became faster (Figure 10, middle panel) and less hindered at the polar interface (labeled by the shallow probes 2- and 3-AS) than that at the deepest positions (probed from 6- to 12-AS). This indicates that the packing of the surfactant acyl chains remained unaffected by the presence of a large water pool (Figure 10, lower panel and Table 4).

The out-of-plane rotation likely corresponds to the slowest nanosecond rotational correlation time. In the absence of water at $w_0 = 0$, it was undistinguishable from the Brownian micelle rotation. The corresponding rotational correlation time value was similar for all probes apart from 12-AS, which was significantly shorter (Figure 10, middle panel and Table 4). When water was added, this rotation became ∼2 times faster for all fluorophore positions.

**MD.** After the equilibration procedure described in Experimental Methods, three runs of MD of AOT/water ($w_0 = 5$) containing each *n*-AS derivative ($n$ = 3-, 7-, and 12-AS) were started over ∼2 ps. The drawing of the *n*-AS probes on Figure 11 was achieved according to the computation, at the end of the simulation, of the distance between the center of mass and some representative atoms of the *n*-AS: the terminal methyl carbon of the stearoyl chain, the carbon of the head carbonyl group, and the carbon of the stearoyl chain connected to the fluorophore. The radial positions of the C3 ester bond on the stearoyl chain of 3-AS were localized in the sulfonate polar group of the AOT surfactant. The ester bond at C12 of 12-AS was close to the end of the surfactant acyl chain, and the 7-AS labeled an intermediate position in the middle of the surfactant acyl chain (Figure 11).

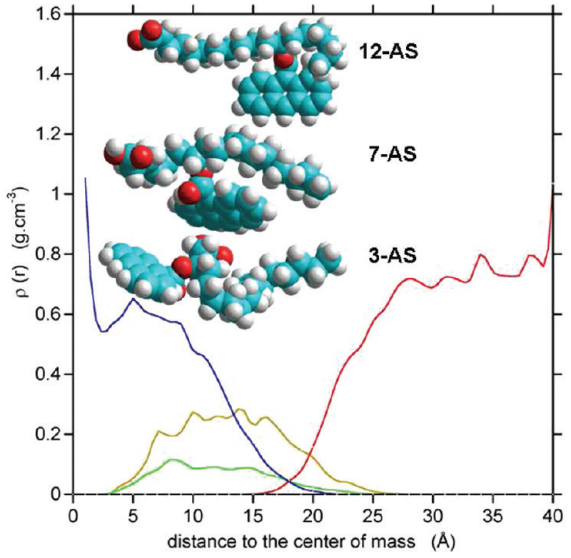


**Figure 11.** Density profile $\rho(r)$ with respect to the center of mass of the micelle; $\rho(r)$ is defined as $\rho_a(r)\, dr = \sum_i \delta(r - r_i) m_i / 4\pi r^2$, where the sum $\sum_i$ extends to a given atom for a given molecule and $\delta(r - r_i)$ is a Dirac function equal to 1 if the given atom (of mass $m_i$) is present in a spherical shell of width = d$r$ at radius $r$, and it is equal to 0 if not.[59] Such a $\rho(r)$ function was computed for the oxygen atom in $H_2O$ (blue line), the carbon 5 atom of iso-octane (red line), the sulfur atom of AOT (yellow line), and the counterion $Na^+$ (green line). The corner effect associated with the use of a cubic box was taken into account for the computation of $\rho_a(r)$.

## DISCUSSION

In this paper, we have provided further insight into the ability of the *n*-AS series of fluorescent probes to sense water content at membrane−water interfaces. This is based on the formation of a specific H-bond between a water molecule and the carbonyl group of the 9-anthroyloxy ester bond at the excited state, leading to efficient fluorescence quenching by nonradiative deactivation, as was previously described.[49] We determined the efficiency of quenching by water of *n*-AS by measuring the excited-state lifetime of *n*-AS in various protic solvents, using the Kamlet−Taft acidity scale.[51,73,74] The calculated quenching rate constant value was ∼5 times larger than that previously published.[49,50] This value is more relevant for describing the water penetration in direct micelles of various detergents. For instance, instead of predicting a relatively high local water concentration of ∼20 M inside of the SDS micellar interior probed by 12-AS,[50] we calculated a much more reduced value of ∼2−4 M, in better agreement with the results of MD simulations describing an essentially water-free hydrocarbon core.[75,76] We therefore quantified the water gradient across RMs of AOT/iso-octane/water using this newly determined


dx.doi.org/10.1021/jp209419y | J. Phys. Chem. B 2012, 116, 1687−1699

water-quenching constant. We also studied the solvatochromic properties of these probes in these RMs, which could provide clues on the water dipolar relaxation dynamics as a function of depth. For this purpose, we delineated the respective contributions of the intramolecular excited-state process with respect to the polar solvent dynamics.

The excited-state lifetime profiles provided by the series of *n*-AS in RMs allowed characterization of the water penetration gradients, which decreased from the shallow 2- and 3-AS derivatives (probing the water−surfactant polar head group interface) to the intermediate ones 7- and 9-AS (probing the surfactant acyl chains close to the branching of the ethyl side chain), in agreement with the 9-anthroyloxy moiety location shown by simulation (Figure 11). The water gradient became steeper with increasing $w_0$. The deepest hydrophobic region of the surfactant hydrocarbon chain probed by 10- and 12-AS remained devoid of water molecules irrespective of the amount of trapped water. The significant penetration of water until approximately the middle of the surfactant hydrocarbon chains may be facilitated on the one hand by the highly dynamic characteristics of RMs. Anisotropy decay experiments of the *n*-AS showed that this occurred over pico- to nanosecond time scales. On the other hand, water penetration may be facilitated by the strong repulsive electrostatic forces between the negatively charged AOT polar head groups. In this respect, a short excited-state lifetime has also been reported for the 12-AS probe incorporated in direct micelles of SDS in water.[50] The strongly negatively charged polar head group of this surfactant probably allowed a highly dynamic state of the acyl chain, thus facilitating some water penetration beyond the hydrated polar region of the micelle. In contrast, a very low degree of water penetration was reported in Triton X-100, an uncharged detergent.[50] This may be due to the stronger packing of the surfactant molecules in these micelles owing to the H-bond network formed between the hydroxyl moieties of their polyoxyethylene polar head groups and water.[77] These observations suggest that in Triton X-100 micelles, water molecules (being mostly involved in a H-bonding network) are mostly unavailable for H-bond formation with foreign molecules such as the *n*-AS. In phospholipid bilayers, the shallower 2-AS probe shows longer excited-state lifetime values than in RMs of high $w_0$.[38−40,50,78−83] This indicates low hydration of the aqueous interface in phospholipidic membranes, consistent with the results obtained by hyperfine splitting measurements of nitroxide probes.[4] The quenching behavior, as a function of the water content $w_0$ in RMs, strongly suggests that it is the available water molecules, and not their total amount, that is important in these quenching experiments. Therefore, only limited amounts of water molecules are available for quenching the 9-anthroyloxy group at membrane−water interfaces, even under 100% hydration conditions.

To use this series of *n*-AS probes to investigate water relaxation dynamics, we attempted to delineate the amplitude of the spectral shift due to the intramolecular relaxation process from that of the polar solvents using various media with different viscosities and polarities. However, the intramolecular relaxation process of the 9-anthroyloxy moiety was extremely fast and was completed in hydrocarbon solvents of low viscosity before ∼50 ps. This is below the limit of the time resolution of our instrument. In high-viscosity hydrocarbon solvents, this intramolecular process was significantly slowed down, consistent with the assumed mechanism involving the relative rotation of the carboxylate group of the C9 ester bond with respect to the anthracene ring. The resulting coplanar conformation of the excited state[42,47] emits at ∼455 nm (a 35 nm red shift with respect to the initial excited-state "perpendicular" conformation). In this configuration, resonance between the $\pi$ electrons of the anthracene ring and those of the carboxyl group occurs. This leads to the occurrence of a CT, characterizing this coplanar state with the negative charge on the carbonyl group oxygen and the positive charge spreading over the aromatic ring. Interaction with polar solvents, even in alcohols of high viscosity (1-hexanol and cyclohexanol), facilitates the formation of the coplanar CT excited state with respect to hydrocarbon solvents. These interactions with the CT excited state led to a further red shift of ∼20 nm in polar protic solvents and ∼10 nm in aprotic ones. Thus, the solvent contribution (dipolar and H-bond interactions) to the total red shift measurable with the 9-anthroyloxy fluorescent derivatives is relatively moderate.

In the absence of water, the TDFSSs in RMs of the *n*-AS series resemble those observed in viscous apolar solvents describing the internal rotational relaxation of the 9-anthroyloxy moiety. In the presence of water, this process occurs on a much faster time scale and is no more measurable for the probes closest to the water AOT interface. Therefore, the TDFSSs are only relevant for the solvent-mediated relaxation processes. The respective amplitudes of the TDFSSs of the shallowest 2-, 3-, 6-, and 7-AS were larger in AOT/water than those in AOT/DMF RMs, showing that both dipolar and H-bond interactions contribute to the relaxation process in the former system. An interaction energy of ∼1 kcal $M^{-1}$ can then be deduced for the H-bond interaction, consistent with a single H-bond between water and the 9-anthroyloxy excited state.[49] In AOT/water RMs, the amplitude of the spectral shift decreased in a depth-dependent way according to the water concentration gradient estimated by lifetime measurements. The water-mediated Stokes shift dynamics was also depth-dependent; it was twice as slow in the middle of the detergent acyl chains as that in the polar head group region. Water does not reach the deepest region of the surfactant acyl chains, as shown by 10- and 12-AS lifetime measurements. Moreover, the TDFSS value observed for the 12-AS is almost the same with or without water in AOT RMs or when DMF replaced water.

We therefore observed, by time-resolved fluorescence in RMs, a slow water-mediated TDFSS reflecting water relaxation kinetics that are several orders of magnitude slower than that in bulk water.[84] This is a common observation made using this technique[9,13,26,45,85,86] as well as in MD simulations.[75,87−89] This slow relaxation has been proposed to be due to the motion of interfacial water in exchange with the bulk,[9,84] to the local dynamics of polar moieties belonging to the macromolecules or their assemblies,[90] or to the mobility of the probes themselves.[91] In the present study, anisotropy decay measurements showed a concordance between the rotational correlation time values and the relaxation times of the water-mediated TDFSS. This was particularly striking for 2- and 3-AS, which were the most sensitive probes to the presence of water. We have already reported for other fluorescent probes such a concordance.[13,26,85] The slow TDFSSs might therefore originate from the correlated motilities of the polar head groups of the surfactant (or *n*-AS probes) and bound water molecules.

## CONCLUSIONS

Our study demonstrates that the specific sensitivity of the excited-state lifetime of the *n*-AS series of probes allows us to

characterize a water concentration gradient in RMs extending from the AOT polar head group up to the middle of the acyl chain. The water concentrations at the membrane−water interface estimated by these probes are low whatever the water-to-surfactant molar ratio as compared to those of the bulk but consistent with those estimated by other techniques.[4] The relatively slow relaxation kinetics of the solvent-induced TDFSS occurring over hundreds of picoseconds up to nanoseconds is likely due to collective relaxation motions of the hydration shell around the fluorescent beacon as well as H-bond formation with the carbonyl group of the 9-anthroate moiety, leading to a partially quenched exciplex.

## AUTHOR INFORMATION

### Corresponding Author

*Tel.: 33-169154842. Fax: 33-169853715. E-mail: mevincent94@yahoo.fr.

## REFERENCES

(1) Disalvo, E. A.; Lairion, F.; Martini, F.; Tymczyszyn, E.; Frias, M.; Almaleck, H.; Gordillo, G. J. *Biochim. Biophys. Acta* **2008**, *1778*, 2655−2670.
(2) Perochon, E.; Lopez, A.; Tocanne, J. F. *Biochemistry* **1992**, *31*, 7672−7682.
(3) Chattopadhyay, A.; Mukherjee, S. *J. Phys. Chem. B* **1999**, *103*, 8180−8185.
(4) Marsh, D. *Eur. Biophys. J. Biophys. Lett.* **2002**, *31*, 559−562.
(5) Marsh, D. *Biophys. J.* **2009**, *96*, 2549−2558.
(6) Eicke, H.-F.; Kvita, P. Reverse micelles and aqueous microphases. In *Reverse Micelles. Biological and Technological Relevance of Amphiphilic Structures in Apolar Media*; Luisi, P. L., Straub, B. E., Eds.; Plenum Press: New York and London, 1984; pp 21−35.
(7) Nicot, C.; Vacher, M.; Vincent, M.; Gallay, J.; Waks, M. *Biochemistry* **1985**, *24*, 7024−7032.
(8) Luisi, P. L.; Giomini, M.; Pileni, M. P.; Robinson, B. H. *Biochim. Biophys. Acta* **1988**, *947*, 209−246.
(9) Bhattacharyya, K.; Bagchi, B. *J. Phys. Chem. A* **2000**, *104*, 10603−10613.
(10) Levinger, N. E. *Science* **2002**, *298*, 1722−1723.
(11) Keh, E.; Valeur, B. *J. Colloid Interface Sci.* **1981**, *79*, 465−468.
(12) Freda, M.; Onori, G.; Paciaroni, A.; Santucci, A. *Phys. Rev. E* **2003**, *68*, 21406−21411.
(13) Vincent, M.; de Foresta, B.; Gallay, J. *Biophys. J.* **2005**, *88*, 4337−4350.
(14) Bhattacharyya, K. *Acc. Chem. Res.* **2003**, *36*, 95−101.
(15) Nicot, C.; Waks, M. *Biotechnol. Genet. Eng. Rev.* **1996**, *13*, 267−314.
(16) Gallay, J.; Vincent, M.; Nicot, C.; Waks, M. *Biochemistry* **1987**, *26*, 5738−5747.
(17) Marzola, P.; Gratton, E. *J. Phys. Chem.* **1991**, *95*, 9488−9495.
(18) Wille, H.; Prusiner, S. B. *Biophys. J.* **1999**, *76*, 1048−1062.
(19) Fiori, S.; Renner, C.; Cramer, J.; Pegoraro, S.; Moroder, L. *J. Mol. Biol.* **1999**, *291*, 163−175.
(20) Orlich, B.; Schomacker, R. *Adv. Biochem. Eng. Biotechnol.* **2002**, *75*, 185−208.
(21) Van Horn, W. D.; Ogilvie, M. E.; Flynn, P. F. *J. Am. Chem. Soc.* **2009**, *131*, 8030−8039.
(22) Parasassi, T.; Di-Stefano, M.; Loiero, M.; Ravagnan, G.; Gratton, E. *Biophys. J.* **1994**, *66*, 763−768.
(23) Viard, M.; Gallay, J.; Vincent, M.; Meyer, O.; Robert, B.; Paternostre, M. *Biophys. J.* **1997**, *73*, 2221−2234.
(24) Sengupta, B.; Guharay, J.; Sengupta, P. K. *Spectrochim. Acta, Part A* **2000**, *56*, 1433−1441.
(25) Lissi, E. A.; Abuin, E. B.; Rubio, M. A.; Ceron, A. *Langmuir* **2000**, *16*, 178−181.
(26) Viard, M.; Gallay, J.; Vincent, M.; Paternostre, M. *Biophys. J.* **2001**, *80*, 347−359.
(27) Correa, N. M.; Levinger, N. E. *J. Phys. Chem. B* **2006**, *110*, 13050−13061.
(28) Beechem, J. M.; Ameloot, M.; Detoma, R. P.; Brand, L. *Biophys. J.* **1985**, *47*, A318−A318.
(29) Waggoner, A. S.; Stryer, L. *Proc. Natl. Acad. Sci. U.S.A.* **1970**, *67*, 579−589.
(30) Podo, F.; Blasie, J. K. *Proc. Natl. Acad. Sci. U.S.A.* **1977**, *74*, 1032−1036.
(31) Thulborn, K. R.; Sawyer, W. H. *Biochim. Biophys. Acta* **1978**, *511*, 125−140.
(32) Blatt, E.; Ghiggino, K. P.; Sawyer, W. H. *J. Chem. Soc., Faraday Trans. 1* **1981**, *77*, 2551−2558.
(33) Blatt, E.; Ghiggino, K. P.; Sawyer, W. H. *Chem. Phys. Lett.* **1985**, *114*, 47−52.
(34) Villalain, J.; Prieto, M. *Chem. Phys. Lipids* **1991**, *59*, 9−16.
(35) De Paillerets, C.; Gallay, J.; Vincent, M.; Rogard, M.; Alfsen, A. *Biochim. Biophys. Acta* **1981**, *644*, 134−142.
(36) Tilley, L.; Thulborn, K. R.; Sawyer, W. H. *J. Biol. Chem.* **1979**, *254*, 2592−2594.
(37) Thulborn, K. R.; Beddard, G. S. *Biochim. Biophys. Acta* **1982**, *693*, 246−252.
(38) Vincent, M.; de Foresta, B.; Gallay, J.; Alfsen, A. *Biochemistry* **1982**, *21*, 708−716.
(39) Vincent, M.; de Foresta, B.; Gallay, J.; Alfsen, A. *Biochem. Biophys. Res. Commun.* **1982**, *107*, 914−921.
(40) Vincent, M.; Gallay, J. *Biochemistry* **1984**, *23*, 6514−6522.
(41) Vincent, M.; Gallay, J.; de Bony, J.; Tocanne, J. F. *Eur. J. Biochem.* **1985**, *150*, 341−347.
(42) Werner, T. C.; Hoffman, R. M. *J. Phys. Chem.* **1973**, *77*, 1611−1615.
(43) Werner, T. C.; Hercules, D. M. *J. Phys. Chem.* **1969**, *75*, 2005−2011.
(44) Thulborn, K. R.; Tilley, L. M.; Sawyer, W. H.; Treloar, F. E. *Biochim. Biophys. Acta* **1979**, *558*, 166−178.
(45) Sykora, J.; Kapusta, P.; Fidler, V.; Hof, M. *Langmuir* **2002**, *18*, 571−574.
(46) Blatt, E.; Ghiggino, K. P.; Sawyer, W. H. *J. Phys. Chem.* **1982**, *86*, 4461−4464.
(47) Matayoshi, E. D.; Kleinfeld, A. M. *Biophys. J.* **1981**, *35*, 215−235.
(48) Berberan-Santos, M. N.; Prieto, M. J. E.; Szabo, A. G. *J. Phys. Chem.* **1991**, *95*, 5471−5475.
(49) Maçanita, A. L.; Costa, F. P.; Costa, S. M. B.; Melo, E. C.; Santos, H. *J. Phys. Chem.* **1989**, *93*, 336−343.
(50) Melo, E. C. C.; Costa, S. M. B.; Maçanita, A. L.; Santos, H. *J. Colloid Interface Sci.* **1991**, *141*, 439−453.
(51) Kamlet, M. J.; Abboud, J. L. M.; Abraham, M. H.; Taft, R. W. *J. Org. Chem.* **1983**, *48*, 2877−2887.
(52) Durantini, A. M.; Falcone, R. D.; Silber, J. J.; Correa, N. M. *ChemPhysChem* **2009**, *10*, 2034−2040.
(53) Livesey, A. K.; Brochon, J. C. *Biophys. J.* **1987**, *52*, 693−706.
(54) Vincent, M.; Brochon, J. C.; Merola, F.; Jordi, W.; Gallay, J. *Biochemistry* **1988**, *27*, 8752−8761.
(55) Vekshin, N.; Vincent, M.; Gallay, J. *Chem. Phys. Lett.* **1992**, *199*, 459−464.
(56) Vincent, M.; Gallay, J. *Eur. Biophys. J.* **1991**, *20*, 183−191.
(57) Burstein, E. A.; Emelyanenko, V. I. *Photochem. Photobiol.* **1996**, *64*, 316−320.
(58) Koti, A. S. R.; Krishna, M. M. G.; Periasamy, N. *J. Phys. Chem. A* **2001**, *105*, 1767−1771.
(59) Abel, S.; Sterpone, F.; Bandyopadhyay, S.; Marchi, M. *J. Phys. Chem. B* **2004**, *108*, 19458−19466.
(60) Brooks, B. R.; Bruccoleri, R. E.; Olafson, B. D.; States, D. J.; Swaminathan, S.; Karplus, M. *J. Comput. Chem.* **1983**, *4*, 187−217.
(61) El Seoud, O. A. *Pure Appl. Chem.* **2009**, *81*, 697−707.
(62) Werner, T. C.; Lyon, D. B. *J. Phys. Chem.* **1982**, *86*, 933−939.
(63) Yamashita, T.; Ushida, T.; Fukushima, T.; Teramae, N. *J. Phys. Chem. B* **2003**, *107*, 4786−4792.
(64) Mukherjee, S.; Sabu, K.; Roy, D.; Mondal, S. K.; Bhattacharyya, K. *Chem. Phys. Lett.* **2004**, *384*, 128−133.

(65) Sykora, J.; Slavicek, P.; Jungwirth, P.; Barucha, J.; Hof, M. *J. Phys. Chem. B* **2007**, *111*, 5869−5877.
(66) Lakowicz, J. R. Dynamics of solvent and spectral relaxation. *Principles of Fluorescence Spectroscopy*; Springer Science: New York, 2006.
(67) Bagchi, B.; Oxtoby, D. W.; Fleming, G. R. *Chem. Phys.* **1984**, *86*, 257−267.
(68) Mudzhikova, G. V.; Brodskaya, E. N. *Colloid J.* **2006**, *68*, 729−737.
(69) Novaira, M.; Moyano, F.; Biasutti, M. A.; Silber, J. J.; Correa, N. M. *Langmuir* **2008**, *24*, 4637−4646.
(70) Visser, A.; Vos, K.; Vanhoek, A.; Santema, J. S. *J. Phys. Chem.* **1988**, *92*, 759−765.
(71) Wittouck, N.; Negri, R. M.; Ameloot, M.; Deschryver, F. C. *J. Am. Chem. Soc.* **1994**, *116*, 10601−10611.
(72) Dutt, G. B. *J. Phys. Chem. B* **2008**, *112*, 7220−7226.
(73) Abboud, J. L. M.; Taft, R. W. *J. Phys. Chem.* **1979**, *83*, 412−419.
(74) Taft, R. W.; Kamlet, M. J. *J. Am. Chem. Soc.* **1976**, *98*, 2886−2894.
(75) Bruce, C. D.; Senapati, S.; Berkowitz, M. L.; Perera, L.; Forbes, M. D. E. *J. Phys. Chem. B* **2002**, *106*, 10902−10907.
(76) Jalili, S.; Akhavan, M. *Colloid Surf., A* **2009**, *352*, 99−102.
(77) Kimura, N.; Umemura, J.; Hayashi, S. *J. Colloid Interface Sci.* **1996**, *182*, 356−364.
(78) Haigh, E. A.; Thulborn, K. R.; Sawyer, W. H. *Biochemistry* **1979**, *18*, 3525−3532.
(79) Hutterer, R.; Schneider, F. W.; Hof, M. *Chem. Phys. Lipids* **1997**, *86*, 51−64.
(80) Pechtold, L. A.; Abraham, W.; Potts, R. O. *J. Invest. Dermatol. Symp. Proc.* **1998**, *3*, 105−109.
(81) Chattopadhyay, A.; Mukherjee, S. *Langmuir* **1999**, *15*, 2142−2148.
(82) Kamo, T.; Nakano, M.; Kuroda, Y.; Handa, T. *J. Phys. Chem. B* **2006**, *110*, 24987−24992.
(83) Shintou, K.; Nakano, M.; Kamo, T.; Kuroda, Y.; Handa, T. *Biophys. J.* **2007**, *93*, 3900−3906.
(84) Pal, S. K.; Zewail, A. H. *Chem. Rev.* **2004**, *104*, 2099−2123.
(85) de Foresta, B.; Gallay, J.; Sopkova, J.; Champeil, P.; Vincent, M. *Biophys. J.* **1999**, *77*, 3071−3084.
(86) Nandi, N.; Bhattacharyya, K.; Bagchi, B. *Chem. Rev.* **2000**, *100*, 2013−2045.
(87) Faeder, J.; Ladanyi, B. M. *J. Phys. Chem. B* **2000**, *104*, 1033−1046.
(88) Harpham, M. R.; Ladanyi, B. M.; Levinger, N. E. *J. Phys. Chem. B* **2005**, *109*, 16891−16900.
(89) Harpham, M. R.; Ladanyi, B. M.; Levinger, N. E.; Herwig, K. W. *J. Chem. Phys.* **2004**, *121*, 7855−7868.
(90) Halle, B.; Nilsson, L. *J. Phys. Chem. B* **2009**, *113*, 8210−8213.
(91) Seidel, M.; Jethwa, J.; Vohringer, P. *Russ. Chem. Bull.* **2004**, *53*, 1471−1476.
(92) Kolling, O. W. *J. Phys. Chem.* **1992**, *96*, 1729−1733.